Journal of Materials Chemistry C

COMMUNICATION

View Article Online
View Journal | View Issue

Cite this: J. Mater. Chem. C, 2018, 6, 4873

Received 13th March 2018,
Accepted 19th April 2018

DOI: 10.1039/c8tc01229f

rsc.li/materials-c

A nonfullerene acceptor utilizing a novel asymmetric multifused-ring core unit for highly efficient organic solar cells†

Chao Li,‡[a] Yuanpeng Xie,‡[a] Bingbing Fan,[a] Guangchao Han,[b] Yuanping Yi *[b] and Yanming Sun *[a]

In this communication, a novel asymmetric ladder-type thiophene-phenylene-thieno[3,2-*b*]thiophene-fused building block TPTT and the corresponding asymmetric nonfullerene acceptor TPTT-IC were reported for the first time. Organic solar cells (OSCs) fabricated with a wide-bandgap polymer PBT1-C as the donor and TPTT-IC as the acceptor yielded a high power conversion efficiency (PCE) of 10.5% with an open-circuit voltage (V_{oc}) of 0.96 V, a short-circuit current (J_{sc}) of 15.6 mA cm^{-2} and a fill factor (FF) of 70%, which is the highest PCE value reported in the literature so far for OSCs based on asymmetric nonfullerene acceptor materials.

Organic solar cells (OSCs), an environmentally benign technology for harvesting solar energy from sunlight to generate electricity, are receiving an increasing amount of attention due to their advantages such as light weight, low cost, mechanic flexibility and solution processibility compared to traditional inorganic solar cells.[1–3] In comparison with the most extensively studied fullerene-based OSCs, recent years have witnessed the rapid development of nonfullerene OSCs. It is well known that nonfullerene acceptors generally feature versatile chemical structure modification, broad absorption in the near-infrared region, tunable molecular energy level and good morphological stability, which can avoid the intrinsic drawbacks derived from fullerene-based acceptors, such as limited structural modulation, restricted optical absorptivity, limited tunability of the frontier energy level and unstable thin film morphology.[4] Benefiting from the rational molecular design of conjugated polymer donors and nonfullerene acceptors as well as the device optimization, remarkable progress has been achieved for OSCs with PCEs over 13%.[5,6] To date, using an acceptor–donor–acceptor (A–D–A) backbone architecture for the design and synthesis of nonfullerene acceptors has proven to be one of the most successful strategies.[5–11] In this A–D–A framework, besides the outer electron accepting (A) unit, the central electron donating (D) core unit also plays an important role in determining the property of the nonfullerene acceptors. Therefore, the design and development of a novel central electron donating core unit to construct A–D–A type nonfullerene acceptors is highly desirable.[12,13]

Among various central electron donating core units, pentacyclic indacenodithiophene (IDT) and heptacyclic indacenodithieno[3,2-*b*]thiophene (IDTT) containing symmetric ladder-type multifused-ring structures are two of the most attractive building blocks for designing high-performance nonfullerene acceptors.[5,8,14] The covalently forced planarization in those two symmetric donor units could not only elongate the effective conjugation length but also facilitate efficient π-electron delocalization. Moreover, the covalently rigidified coplanar structures could prevent the rotational disorder, reduce the reorganization energy and enhance the intrinsic charge carrier mobility. In addition, these two symmetric donor units functionalized with saturated carbons at the bridging position could circumvent the infusibility without disrupting the backbone π-conjugation.[15] Since Zhan *et al.*[7] firstly reported the A–D–A type nonfullerene acceptor ITIC using a symmetric IDTT building block as the central electron donating core unit, much effort has been devoted towards modifying the molecular structures of these two symmetric donor units, including side chain engineering,[6,16–19] backbone conjugation regulation,[20,21] heteroatom substitution,[22] π-bridge modulation,[23–25] *etc.* These modified donor units generally contain symmetric structures and effectively promote the development of nonfullerene OSCs. However, we noticed that there have been limited attempts to modify these two symmetric donor units to be asymmetric donor units.[26] The incorporation of an asymmetric ladder-type multifused-ring core unit into an A–D–A type nonfullerene acceptor is of great interest in the material development of nonfullerene OSCs, but synthetically less explored. In addition, the design and development of highly efficient nonfullerene acceptors based on an asymmetric ladder-type multifused-ring core unit may be meaningful for advancing and diversifying nonfullerene acceptors.

[a] Heeger Beijing Research and Development Center, School of Chemistry, Beihang University, Beijing 100191, China. E-mail: sunym@buaa.edu.cn
[b] Beijing National Laboratory for Molecular Science, Key Laboratory of Organic Solids, Institute of Chemistry, Chinese Academy of Sciences, Beijing 100190, P. R. China. E-mail: ypyi@iccas.ac.cn

† Electronic supplementary information (ESI) available. See DOI: 10.1039/c8tc01229f
‡ These two authors contributed equally to this work.

In this communication, we firstly designed and synthesized a novel asymmetric ladder-type thiophene-phenylene-thieno-[3,2-*b*]thiophene-fused building block TPTT. Unlike an IDT unit where the central phenylene is connected with two outer thiophene units, and an IDTT unit where the central phenylene is connected with two outer thieno[3,2-*b*]thiophene units through two embedded cyclopentadienyl moieties, this TPTT unit integrates the thiophene, phenylene and thieno[3,2-*b*]thiophene units into a single fused molecular entity. This thiophene-phenylene-thieno[3,2-*b*]thiophene-fused molecular arrangement makes the TPTT building block an asymmetric structure, which is very different from the symmetric structures of the IDT and IDTT building blocks. On the other hand, in comparison with the symmetric IDT and IDTT units, the π-conjugation length, fused ring numbers and electron-donating ability of the TPTT unit are in between the two materials. Therefore, based on the aforementioned properties, it is highly desirable to construct an A–D–A type nonfullerene acceptor using the TPTT unit. Herein, we reported a novel asymmetric nonfullerene acceptor TPTT-IC using this asymmetric TPTT building block as the central donating core unit and 1,1-dicyanomethylene-3-indanone (IC) as the outer accepting unit. It was found that TPTT-IC exhibits strong and broad absorption in the long wavelength range from 500 to 800 nm and an appropriate lowest unoccupied molecular orbital (LUMO) energy level. By blending TPTT-IC with a wide-bandgap polymer donor PBT1-C,[27] OSCs showed a high PCE of 10.5%, with an open-circuit voltage (V_{oc}) of 0.96 V, a short-circuit current (J_{sc}) of 15.6 mA cm^{-2} and a fill factor (FF) of 70%. To the best of our knowledge, the PCE of 10.5% is so far the best efficiency reported in the literature for OSCs using asymmetric nonfullerene acceptor materials.[26,28,29] These results indicate that this asymmetric TPTT building block is a promising central electron donating core unit for constructing high-performance A–D–A type nonfullerene acceptors.

The synthetic route of TPTT-IC is shown in Scheme 1 and the detailed experimental procedures are outlined in the ESI.† With a Stille coupling reaction, diethyl 2,5-dibromoterephthalate was reacted with tributyl(thiophen-2-yl)stannane to get compound **1**, which was treated with tributyl(thieno[3,2-*b*]thiophen-2-yl)stannane to obtain compound **2**. Double nucleophilic addition of compound **2** with 4-hexylphenyllithium led to two benzyl alcohols, which were then subjected to intramolecular Friedel–Crafts cyclization under acidic conditions to afford the novel asymmetric ladder-type multifused-ring building block TPTT. This hexacyclic arene TPTT was then lithiated by *n*-butyllithium followed by quenching with *N*-formylpiperidine to obtain the dialdehyde compound TPTT-CHO, which was finally reacted with IC through Knoevenagel condensation reaction to yield the target nonfullerene acceptor TPTT-IC. All these new compounds were fully characterized using ^{1}H NMR and ^{13}C NMR spectroscopy, GCMS and HRMS (ESI†). The TPTT-IC exhibited good solubility in common organic solvents such as chloroform, tetrahydrofuran, chlorobenzene, *etc.*

The molecular geometry of TPTT-IC was optimized by DFT at the ωB97XD/6-31G** level and the alkyl chains are replaced by a methyl group for simplicity. The TPTT-IC has an asymmetric (its permanent dipole moment is about 6.1 D) and planar structure (Fig. S1a, ESI†). The calculated (tuned-ωB97XD/6-31G**) frontier molecular orbital profiles and energy levels of TPTT-IC are shown in Fig. 1a. The first excited state (S1) of TPTT-IC is mainly from the highest occupied molecular orbital (HOMO) to LUMO (86.3%) and HOMO−1 to LUMO+1 (9.0%) transitions. The vertical excitation energy of S1 is 2.31 eV in the gas phase (f = 2.51). Note that the energy gap between the LUMO+1 and LUMO is only 0.32 eV, indicating that the LUMO+1 of TPTT-IC can accept electrons from the LUMO of the polymer donor.[30] The LUMO of TPTT-IC is delocalized over the entire molecular backbone, which would be beneficial for electron transport, while the HOMO of TPTT-IC is mainly located on the central TPTT core. Due to the sterically hindered side chains on the core, the dominant transport channels for TPTT-IC can be formed by the local intermolecular π–π stacking between the terminal electron-withdrawing units (IC).[31] The optimized molecular geometries of TPTT-IC dimers and their corresponding intermolecular binding energies calculated under the correction of basis set superposition error (BSSE) are shown in Fig. 1b, and the intermolecular binding energies of ITIC dimers are also calculated for comparison (Fig. S1b, ESI†).

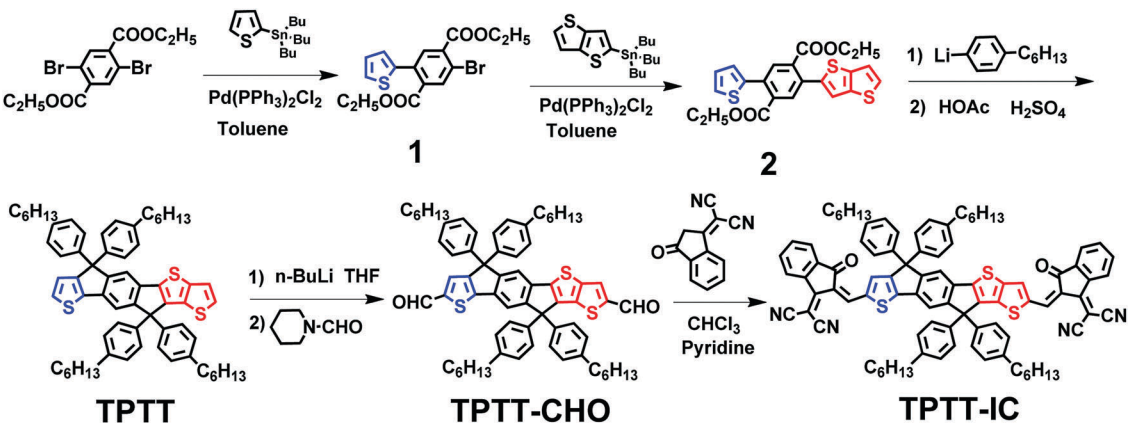

Scheme 1 Synthetic route of TPTT-IC.

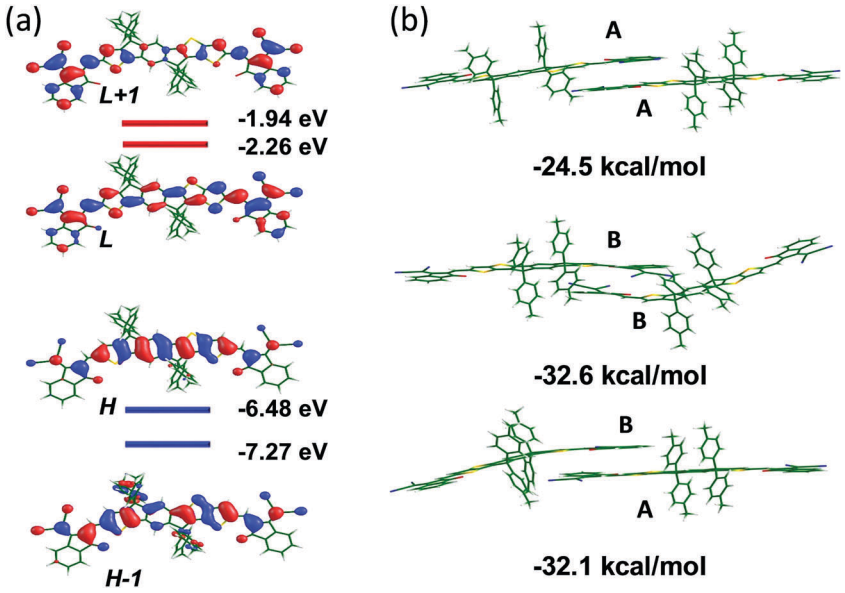

Fig. 1 (a) Frontier molecular orbitals and the corresponding energy levels of TPTT-IC and (b) optimized geometries of TPTT-IC dimers and the corresponding intermolecular binding energies by DFT calculations.

In comparison with the symmetric ITIC structure, there are three kinds of packing modes by terminal π–π stacking for TPTT-IC due to the asymmetric structure. Two of them (with similar binding energies and more stable configurations) have much stronger intermolecular interactions than that of ITIC, suggesting that the electron mobility of TPTT-IC would be higher than that of ITIC.

The UV-visible absorption spectra of TPTT-IC and ITIC in dilute chloroform solution and thin films are provided in Fig. S2 (ESI†) and Fig. 2b, respectively, and the related data are summarized in Table S1 (ESI†). In the dilute chloroform solution, the TPTT-IC exhibited a maximum absorption peak at 668 nm and an obvious shoulder peak at 618 nm. From solution to the solid state, the TPTT-IC thin film showed a broader absorption range and a maximum absorption peak shifted from 668 to 692 nm, suggesting strong intermolecular interactions of TPTT-IC in the solid state. Compared with the symmetric star molecule ITIC, TPTT-IC exhibited a slightly blue-shifted absorption both in solution and the solid state, which could be attributed to the weaker electron-donating ability and shorter π-conjugation length of the asymmetric TPTT unit than that of the symmetric IDTT unit. According to the absorption edge of TPTT-IC and ITIC thin films, the optical bandgaps of TPTT-IC and ITIC were calculated to be 1.63 and 1.60 eV, respectively. Since the absorption wavelength region of the wide-bandgap polymer donor PBT1-C thin film mainly centered at 400–600 nm, both the asymmetric TPTT-IC acceptor and the symmetric ITIC acceptor had a complementary absorption with the PBT1-C donor, which would be beneficial for enhancing light harvesting so as to obtain a high J_{sc} of the organic solar cells.

Cyclic voltammetry (CV) measurements were conducted to evaluate the electrochemical properties of TPTT-IC and ITIC. The CV curves of TPTT-IC and ITIC are provided in Fig. S2 (ESI†) and the corresponding CV data are collected in Table S1 (ESI†). The onset oxidation potential of the ferrocene external

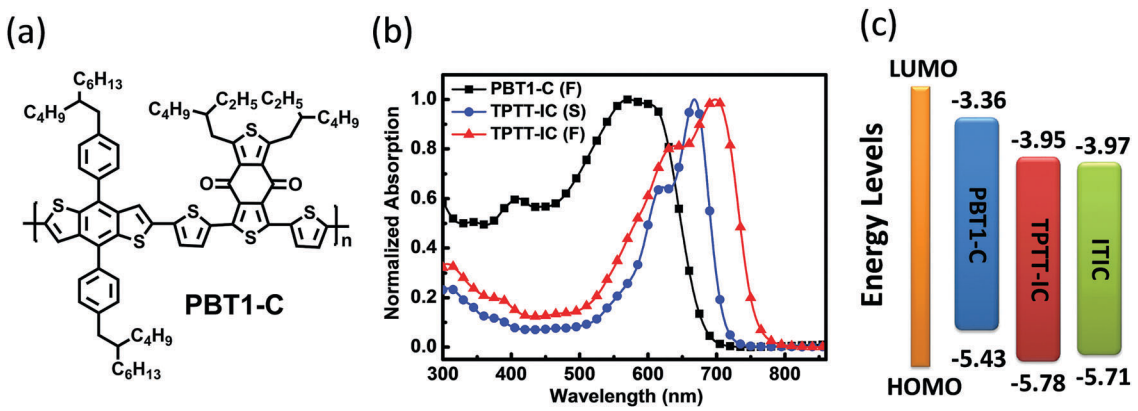

Fig. 2 (a) Chemical structure of PBT1-C, (b) absorption spectra of PBT1-C (film), TPTT-IC (solution) and TPTT-IC (film) and (c) energy level diagram.

standard was determined to be 0.43 eV. The onset oxidation and reduction potentials of the TPTT-IC and ITIC were measured to be 1.41 and 1.34 and −0.42 and −0.34 V (*vs.* Ag/Ag^+), respectively, and the corresponding HOMO and LUMO energy levels of the TPTT-IC and ITIC films were estimated to be −5.78, −5.71 and −3.95, −3.97 eV, respectively. The relatively lower HOMO energy level of TPTT-IC in comparison with ITIC could be ascribed to the less electron-rich nature of the TPTT unit than that of the IDTT unit. The energy level diagram relative to the vacuum level is shown in Fig. 2c. The energy level offset between the HOMO of the polymer donor PBT1-C and the LUMO of the nonfullerene acceptor TPTT-IC and ITIC were calculated to be 1.48 and 1.46 eV, respectively, which are expected to achieve a high V_{oc} in organic solar cells.

To evaluate the photovoltaic performance of TPTT-IC, bulk heterojunction (BHJ) OSCs with an inverted structure of ITO/ZnO/PBT1-C:TPTT-IC/MoO_3/Ag were fabricated. The active layer was prepared by spin-coating in a chloroform solution with a PBT1-C:TPTT-IC weight ratio of 1 : 1 and then thermally annealed at 100 °C for 10 minutes. Without DIO, the OSCs showed a PCE of 7.1% with a V_{oc} of 0.98 V, a J_{sc} of 12.9 mA cm^{-2}, and a FF of 56.2%. The high V_{oc} value was attributed to the large energy offset between the HOMO of PBT1-C and the LUMO of TPTT-IC. With an increase of the DIO content, the OSCs showed much better photovoltaic performance with improved J_{sc} and FF values accompanied by a slight decrease of the V_{oc} value. When 0.5% DIO was used, the OSCs achieved a high PCE of 10.0% with a V_{oc} of 0.96 V, a J_{sc} of 15.0 mA cm^{-2} and a FF of 69.5%. The effect of thin film thickness on the photovoltaic performance of OSCs was also investigated. It was found that when the thin film thickness was 103 nm, the OSCs obtained an optimal PCE of 10.5% with a V_{oc} of 0.96 V, a J_{sc} of 15.6 mA cm^{-2} and a FF of 70%. In comparison, the PBT1-C:ITIC device delivered a slightly lower photovoltaic performance with a PCE of 10.2% accompanied by a V_{oc} of 0.97 V, a J_{sc} of 15.0 mA cm^{-2} and a FF of 69.7%. The *J*–*V* curves of the optimized devices are presented in Fig. 3a, and the related device characteristics are summarized in Tables S3 and S4 (ESI†). The histogram of the PCE measurements for 30 ITIC- and TPTT-IC-based devices is shown in Fig. S3 (ESI†). Moreover, the operational stability of the PBT1-C:ITIC and PBT1-C:TPTT-IC devices was tested (Fig. S4, ESI†). It was found that the TPTT-IC-based devices showed better operational stability than those of ITIC-based solar cells and still maintained more than 80% of the original PCE values after continuous measurements under light for 10 min.

The corresponding incident-photon-to-current efficiency (IPCE) spectrum of the optimum PBT1-C:TPTT-IC based device (Fig. 3b) covers a broad wavelength extending from 300 to 800 nm with a maximum IPCE value of 75.8% at 550 nm, which was higher than the maximum IPCE value of the optimal PBT1-C:ITIC device. The IPCE spectrum ranging from 650 to 800 nm was derived from the absorption of nonfullerene acceptor TPTT-IC, while that in the 300–650 nm range was originated from the absorption of polymer donor PBT1-C. The J_{sc} value calculated from integration of the IPCE spectra is 15.01 mA cm^{-2} and 14.67 mA cm^{-2} for the optimum PBT1-C:TPTT-IC and PBT1-C:ITIC devices, respectively, which is consistent with the value obtained from the *J*–*V* curves within 5% mismatch, demonstrating that the photovoltaic experiments were reliable.

To investigate the charge transport properties of the TPTT-IC and PBT1-C:TPTT-IC blends, the space charge limited current (SCLC) method was performed to evaluate electron and hole mobilities by fabricating electron-only devices with a structure of ITO/ZnO/PBT1-C:acceptor/ZrAcac/Al and hole-only devices with a structure of ITO/PEDOT:PSS/PBT1-C:acceptor/MoO_3/Ag (Fig. S5 and S6, ESI†). The device based on pure TPTT-IC exhibited an electron mobility of 4.3×10^{-4} cm^2 V^{-1} s^{-1}, while the ITIC-based device showed a relatively lower electron mobility of 2.8×10^{-4} cm^2 V^{-1} s^{-1}, which was in agreement with DFT calculations that the TPTT-IC molecules have a higher binding energy than the ITIC molecules. The PBT1-C:TPTT-IC blend device presented a hole mobility of 5.1×10^{-4} cm^2 V^{-1} s^{-1} and an electron mobility of 3.23×10^{-4} cm^2 V^{-1} s^{-1} (μ_h/μ_e ratio = 1.58), while the PBT1-C:ITIC device gave a lower hole mobility of 4.9×10^{-4} cm^2 V^{-1} s^{-1} and a lower electron mobility of 2.85×10^{-4} cm^2 V^{-1} s^{-1} (μ_h/μ_e = 1.72). The higher and more balanced hole and electron mobilities of the PBT1-C:TPTT-IC blend would be beneficial for obtaining the higher J_{sc} and higher FF values of the organic solar cells. The related data are summarized in Table S2 (ESI†).

The morphology of the optimal blend films was studied using atomic force microscopy (AFM). As shown in Fig. S7 (ESI†), the PBT1-C:TPTT-IC blend film presented a root-mean-square (RMS) roughness value of 2.47 nm, which was higher than that of the

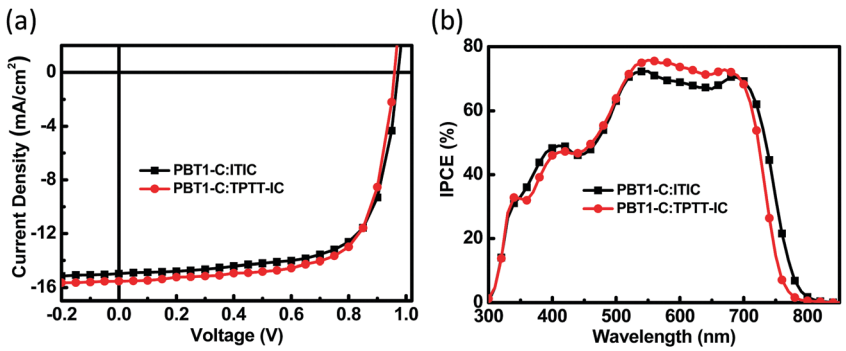

Fig. 3 (a) *J*–*V* curves of the PBT1-C:ITIC and PBT1-C:TPTT-IC devices and (b) the corresponding IPCE curves.

Table 1 Device data of optimized OSCs based on the PBT1-C:acceptor

Acceptor	J_{sc}[a] (mA cm^{-2})	$J_{sc,cal}$ (mA cm^{-2})	V_{oc}[a] (V)	FF[a] (%)	PCE[a] (%)
TPTT-IC	15.5 ± 0.4	15.01	0.96 ± 0.01	69.4 ± 1.4	10.3 (10.5)
ITIC	14.9 ± 0.2	14.67	0.97 ± 0.01	69.0 ± 1.1	10.0 (10.2)

[a] Average values with standard deviation were obtained from 10 devices.

PBT1-C:ITIC blend. The PBT1-C:TPTT-IC and PBT1-C:ITIC blend films all showed an obvious fiber network structure, which can be seen from their height and phase images. This favorable morphology was helpful for charge transport, thus leading to high PCEs for both the PBT1-C:TPTT-IC and PBT1-C:ITIC OSCs devices (Table 1).

In summary, a new A–D–A type nonfullerene acceptor TPTT-IC using a novel asymmetric ladder-type multifused-ring TPTT building block as the central electron donating core unit and IC as the outer accepting unit was designed and synthesized. The TPTT-IC possessed a planar and asymmetric molecular structure, high electron transporting properties, strong and broad absorption in the visible region, and an appropriate LUMO energy level. By blending the nonfullerene acceptor TPTT-IC with a wide-bandgap polymer donor PBT1-C, the OSCs exhibited an outstanding PCE of 10.5% with a V_{oc} of 0.96 V, a J_{sc} of 15.6 mA cm^{-2} and a FF of 70%, which is higher than that of the ITIC-based device. This work demonstrates a new strategy for the development of high-performance A–D–A type acceptor materials using the asymmetric ladder-type multifused-ring donating core unit.

Conflicts of interest

There are no conflicts to declare.

Acknowledgements

The authors greatly appreciate the financial support from the National Natural Science Foundation of China (No. 51473009, 21674007, 21734001).

Notes and references

1 Y. Li, *Acc. Chem. Res.*, 2012, **45**, 723–733.
2 Y. Cai, L. Huo and Y. Sun, *Adv. Mater.*, 2017, **29**, 1605437.
3 D. Baran, R. S. Ashraf, D. A. Hanifi, M. Abdelsamie, N. Gasparini, J. A. Röhr, S. Holliday, A. Wadsworth, S. Lockett, M. Neophytou, C. J. M. Emmott, J. Nelson, C. J. Brabec, A. Amassian, A. Salleo, T. Kirchartz, J. R. Durrant and I. McCulloch, *Nat. Mater.*, 2016, **16**, 363.
4 Y. Lin and X. Zhan, *Mater. Horiz.*, 2014, **1**, 470–488.
5 W. Zhao, S. Li, H. Yao, S. Zhang, Y. Zhang, B. Yang and J. Hou, *J. Am. Chem. Soc.*, 2017, **139**, 7148–7151.
6 Z. Fei, F. D. Eisner, X. Jiao, M. Azzouzi, J. A. Röhr, Y. Han, M. Shahid, A. S. R. Chesman, C. D. Easton, C. R. McNeill, T. D. Anthopoulos, J. Nelson and M. Heeney, *Adv. Mater.*, 2018, **30**, 1705209.
7 Y. Lin, J. Wang, Z.-G. Zhang, H. Bai, Y. Li, D. Zhu and X. Zhan, *Adv. Mater.*, 2015, **27**, 1170–1174.
8 D. Xie, T. Liu, W. Gao, C. Zhong, L. Huo, Z. Luo, K. Wu, W. Xiong, F. Liu, Y. Sun and C. Yang, *Solar RRL*, 2017, **1**, 1700044.
9 C. Yan, S. Barlow, Z. Wang, H. Yan, A. K. Y. Jen, S. R. Marder and X. Zhan, *Nat. Rev. Mater.*, 2018, **3**, 18003.
10 T. Li, S. Dai, Z. Ke, L. Yang, J. Wang, C. Yan, W. Ma and X. Zhan, *Adv. Mater.*, 2018, **30**, 1705969.
11 J. Zhu, Z. Ke, Q. Zhang, J. Wang, S. Dai, Y. Wu, Y. Xu, Y. Lin, W. Ma, W. You and X. Zhan, *Adv. Mater.*, 2018, **30**, 1704713.
12 Z. Zhang and X. Zhu, *Chem. Mater.*, 2018, **30**, 587–591.
13 H. Wu, H. Fan, S. Xu, C. Zhang, S. Chen, C. Yang, D. Chen, F. Liu and X. Zhu, *Solar RRL*, 2017, **1**, 1700165.
14 Q. Fan, Y. Wang, M. Zhang, B. Wu, X. Guo, Y. Jiang, W. Li, B. Guo, C. Ye, W. Su, J. Fang, X. Ou, F. Liu, Z. Wei, T. C. Sum, T. P. Russell and Y. Li, *Adv. Mater.*, 2018, **30**, 1704546.
15 J.-S. Wu, S.-W. Cheng, Y.-J. Cheng and C.-S. Hsu, *Chem. Soc. Rev.*, 2015, **44**, 1113–1154.
16 Y. Lin, Q. He, F. Zhao, L. Huo, J. Mai, X. Lu, C.-J. Su, T. Li, J. Wang, J. Zhu, Y. Sun, C. Wang and X. Zhan, *J. Am. Chem. Soc.*, 2016, **138**, 2973–2976.
17 Y. Lin, F. Zhao, Q. He, L. Huo, Y. Wu, T. C. Parker, W. Ma, Y. Sun, C. Wang, D. Zhu, A. J. Heeger, S. R. Marder and X. Zhan, *J. Am. Chem. Soc.*, 2016, **138**, 4955–4961.
18 Y. Yang, Z.-G. Zhang, H. Bin, S. Chen, L. Gao, L. Xue, C. Yang and Y. Li, *J. Am. Chem. Soc.*, 2016, **138**, 15011–15018.
19 X. Liu, B. Xie, C. Duan, Z. Wang, B. Fan, K. Zhang, B. Lin, F. J. M. Colberts, W. Ma, R. A. J. Janssen, F. Huang and Y. Cao, *J. Mater. Chem. A*, 2018, **6**, 395–403.
20 S. Dai, F. Zhao, Q. Zhang, T.-K. Lau, T. Li, K. Liu, Q. Ling, C. Wang, X. Lu, W. You and X. Zhan, *J. Am. Chem. Soc.*, 2017, **139**, 1336–1343.
21 B. Kan, H. Feng, X. Wan, F. Liu, X. Ke, Y. Wang, Y. Wang, H. Zhang, C. Li, J. Hou and Y. Chen, *J. Am. Chem. Soc.*, 2017, **139**, 4929–4934.
22 Y. Li, L. Zhong, F.-P. Wu, Y. Yuan, H.-J. Bin, Z.-Q. Jiang, Z. Zhang, Z.-G. Zhang, Y. Li and L.-S. Liao, *Energy Environ. Sci.*, 2016, **9**, 3429–3435.
23 F. Liu, Z. Zhou, C. Zhang, J. Zhang, Q. Hu, T. Vergote, F. Liu, T. P. Russell and X. Zhu, *Adv. Mater.*, 2017, **29**, 1606574.
24 Y. Cui, C. Yang, H. Yao, J. Zhu, Y. Wang, G. Jia, F. Gao and J. Hou, *Adv. Mater.*, 2017, **29**, 1703080.
25 P. Ye, Y. Chen, J. Wu, X. Wu, S. Yu, W. Xing, Q. Liu, X. Jia, A. Peng and H. Huang, *J. Mater. Chem. C*, 2017, **5**, 12591–12596.
26 S. Feng, C. Zhang, Y. Liu, Z. Bi, Z. Zhang, X. Xu, W. Ma and Z. Bo, *Adv. Mater.*, 2017, **29**, 1703527.
27 T. Liu, L. Huo, S. Chandrabose, K. Chen, G. Han, F. Qi, X. Meng, D. Xie, W. Ma, Y. Yi, J. M. Hodgkiss, F. Liu, J. Wang, C. Yang and Y. Sun, *Adv. Mater.*, 2018, 1707353.
28 Z. Kang, S.-C. Chen, Y. Ma, J. Wang and Q. Zheng, *ACS Appl. Mater. Interfaces*, 2017, **9**, 24771–24777.
29 C. Tang, S.-C. Chen, Q. Shang and Q. Zheng, *Sci. China Mater.*, 2017, **60**, 707–716.
30 A. Kuzmich, D. Padula, H. Ma and A. Troisi, *Energy Environ. Sci.*, 2017, **10**, 395–401.
31 G. Han, Y. Guo, X. Song, Y. Wang and Y. Yi, *J. Mater. Chem. C*, 2017, **5**, 4852–4857.